Bulk and surface spin waves of the superantiferromagnetic ground-state Heisenberg system

1997 J. Phys.: Condens. Matter 9 2915

(http://iopscience.iop.org/0953-8984/9/14/007)

J. Phys.: Condens. Matter **9** (1997) 2915–2930. Printed in the UK PII: S0953-8984(97)76659-1

Bulk and surface spin waves of the superantiferromagnetic ground-state Heisenberg system

M Tamine

Laboratoire de Physique de L'Etat Condensé, Unité de Recherche Associée au CNRS No 807, Faculté des Sciences, Université du Maine, F-72017 Le Mans Cédex, France

Received 24 July 1996, in final form 20 November 1996

Abstract. A formalism for calculating the bulk and surface spin waves in the ground-state frustrated superantiferromagnetic Heisenberg system is presented. The magnetic structure consists of semi-infinite ferromagnetic chains which are antiferromagnetically coupled. The surface spin-wave theory introducing the matching method is used to calculate the energy of the surface magnon. The magnon dispersion curve is calculated as a function of the frustration parameter $J_{AB}^{1v}/J_{AA(BB)}^{2v}$ and the bulk–surface exchange ratio $\varepsilon_{ij}^{1v\|} = J_{AB}^{1vs}/J_{AB}^{1v}$. The behaviour of the bulk magnon as well as the acoustic and optical surface modes which are found to be very sensitive to the surface exchange and anisotropy are interpreted by means of a $J_{AB}^{1v}/J_{AA(BB)}^{2v}$ ratio. The results show that a high instability of bulk and surface spin precession occurs for $0 < J_{AB}^{1v}/J_{AA(BB)}^{2v} \leqslant 4$, and disappears for $J_{AB}^{1v}/J_{AA(BB)}^{2v} = 4$. The latter value corresponds to an antiferromagnetic arrangement of the ground state.

1. Introduction

There have been an increasing number of investigations dealing with uniformly frustrated systems. These systems, which are periodically defined, have been given exact treatments, using different approximations [1–3]. Apart from the evident theoretical interest, uniformly frustrated systems can be found in real physical systems such as antiferromagnetic FCC alloys and arrays of planar Josephson junctions in transverse magnetic fields [4]. In other respects, numerous 2D and 3D geometrically frustrated magnetic structures have been widely investigated during the last decade from both the experimental and the theoretical points of view, as reported in the literature (see for example [5]). Examples of this behaviour are exhibited by 3d-transition-metal oxides [6, 7] and fluorides [8, 9]. In some crystalline compounds, one or several paramagnetic ions build up cationic triangles; so the antiferromagnetic nature of the superexchange interactions or the presence of single-ion anisotropy leads to non-collinear magnetic configurations at absolute zero because of geometrical magnetic frustration [7–9].

In spite of a collinear magnetic configuration, it has been suggested that magnetic frustration may occur in simple cubic antiferromagnets such as MF_3 (M = Cr, Fe, V, ...). This frustration originates from the competition of antiferromagnetic exchange interactions between the first- (J_{AB}^{1v}) inter-sublattice nearest and the second- ($J_{AA(BB)}^{2v}$) intra-sublattice next-nearest neighbours. This behaviour was recently confirmed by computer simulations, and different types of magnetic configuration were evident at absolute zero, associated with two domains of values of $J_{AB}^{1v}/J_{AA(BB)}^{2v}$ [10]. The constraint function F_c which estimates the degree of magnetic frustration is defined by comparing the magnetic energy (E_c), which

0953-8984/97/142915+16$19.50

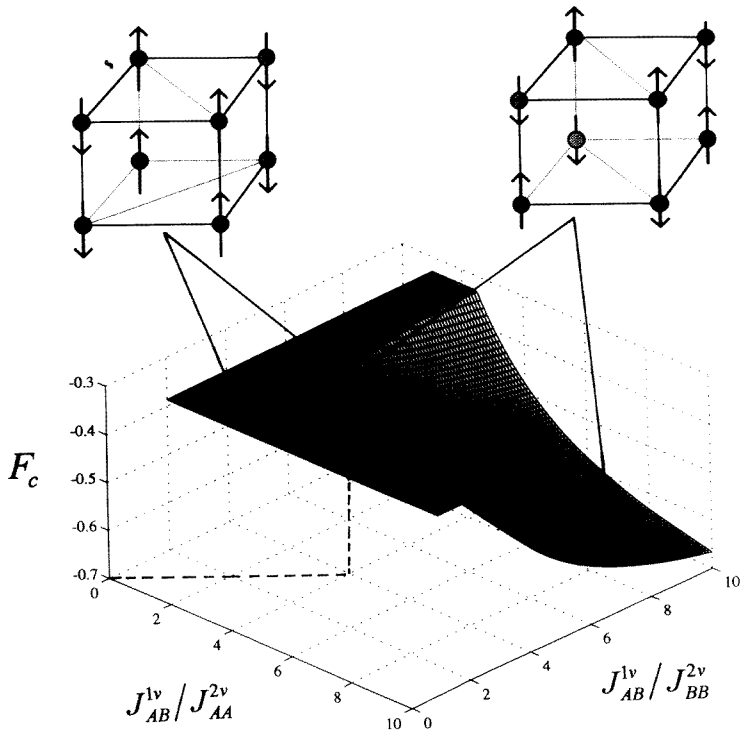

Figure 1. Magnetic configurations established at $T = 0$ corresponding to the constraint function F_c plotted with $|S_A| = |S_B| = 5/2$ as a function of $[J_{AB}^{1v}/J_{AA}^{2v}, J_{AB}^{1v}/J_{BB}^{2v}]$ in the basal plane.

results from the system of interacting spins, to the energy (E_b) calculated for the same magnetic system assuming non-frustrated interactions. The expression is given as follows:

$$F_c = -\frac{E_c}{E_b} = -\left(\sum_{\langle i,j\rangle} J_{AB}^{1v} S_i^{(A)} S_j^{(B)} + \sum_{\langle i,i'\rangle} J_{AA}^{2v} S_i^{(A)} S_{i'}^{(A)} + \sum_{\langle j,j'\rangle} J_{BB}^{2v} S_j^{(B)} S_{j'}^{(B)}\right) \times \left(\sum_{\langle i,j\rangle} |J_{AB}^{1v}||S_i^{(A)}||S_j^{(B)}| + \sum_{\langle i,i'\rangle} |J_{AA}^{2v}||S_i^{(A)}||S_{i'}^{(A)}| + \sum_{\langle j,j'\rangle} |J_{BB}^{2v}||S_j^{(B)}||S_{j'}^{(B)}|\right)^{-1}. \tag{1.1}$$

The function F_c is plotted in figure 1.

Let us recall you briefly the most significant results.

(i) For $J_{AB}^{1v}/J_{AA(BB)}^{2v} > 4$ (the domain where F_c tends asymptotically to -1), the magnetic configuration corresponds to that in a frustrated cubic antiferromagnet ground state: the magnetic exchange interactions between the first neighbours are satisfied whereas those between the second-nearest neighbours are not.

(ii) For $0 < J_{AB}^{1v}/J_{AA(BB)}^{2v} \leqslant 4$ (the domain where $F_c = -1/3$), the magnetic structure results in ferromagnetic chains which are antiferromagnetically coupled—the so-called ground-state superantiferromagnetic arrangement—for which evidence was recently reported from the 2D Heisenberg model [11].

So far, to our knowledge, no study has been reported on bulk and surface spin waves in

this magnetic configuration. This has motivated the present work.

From a theoretical point of view, one of the calculation methods successfully used on the magnetic properties of surfaces and resonances is the matching method [12]. This approach makes use of secular equations of spin motion established for the bulk of the semi-infinite magnetic system, which is shown to contain all of the information concerning travelling modes, as well as evanescent modes, in the direction perpendicular to the magnetic surface. The eigenvalue matrix is derived from the Heisenberg Hamiltonian, and the energies of the localized states for the surface magnons are obtained using this method, which consists in matching the properties of bulk magnons with evanescent spin waves on the surface. The existence, the nature and the shape of the solutions are discussed in terms of surface exchange parameters, by taking into account the results of simulation.

Firstly, in next section we present the bulk dynamical properties, and the surface spin-wave eigenvalue equation is derived using the random-phase approximation. Then, in section 3 the theory of the matching procedure method used in order to describe the localized energy states of surface magnons is developed. The bulk and surface spin-wave spectra are discussed in section 4, and concluding remarks are summarized in section 5.

2. Bulk dynamical properties

The qualitative features of surface spin waves can be easily illustrated using the (001) face of the simple cubic structure. The crystal is assumed to be infinite in the x- and y-directions and extended from $z = 0$ to $z = \infty$. The coordinate system for the (001) surface is illustrated in figure 2. The z-axis is chosen as the inward normal to the surface, whereas the x–y plane is always parallel to the surface plane. Layers which are parallel to the surface are numbered initially, the surface being considered as the first layer. Beyond the second layer, all of the exchange interactions have the bulk value $J_{AB}^{1(2)v}(i, j)$ for antiferromagnetic inter-sublattice (A–B) nearest and next-nearest neighbours, and $J_{AA(BB)}^{1v}(i, i(j, j))$ for ferromagnetic intra-sublattice (A–A (B–B)) nearest neighbours only. The nearest- and the next-nearest-neighbour exchange interactions between spins on the surface are respectively described by $J_{AB}^{1vs}(i, j)$ and $J_{AA(BB)}^{2vs}(i, i(j, j))$, and the interactions between the first and second layers by $J_{AB}^{2v\perp}(i, j)$ and $J_{AA(BB)}^{1v\perp}(i, i(j, j))$.

The general exchange Hamiltonian for two interpenetrating ferromagnetic sublattices A and B extended to the second-nearest-neighbour exchange interactions including the Zeeman effect is expressed as

$$H = \sum_{\langle i,j\rangle} J_{AB}^{1(2)v}(i, j) S_i^{(A)} S_j^{(B)} + \sum_{\langle i,i'(j,j')\rangle} J_{AA(BB)}^{1(2)v}(i, i'(j, j')) S_{i(j)}^{A(B)} S_{i'(j')}^{A(B)} + \mu^{A(B)} H_{(n)}^{A(B)} \sum_{\langle i,(j)\rangle} S_{i(j)}^{A(B)}. \tag{2.1}$$

Here, $\mu^{A(B)} = g\mu_b$ are the gyromagnetic ratios for ions on A and B sublattices respectively. i and i' run over the sublattice A sites only, j and j' over the sublattice B sites only. $H_{(n)}^{A(B)} = H_0 + H_{a(n)}^{A(B)}$ are effective fields experienced by the ions on the A and B sublattices respectively, and are due to the externally applied field H_0 and to the effective anisotropy fields $H_{a(n)}^{A(B)}$ acting on the nth layer. They are taken to lie along the easy direction of magnetization, which itself is taken to be the direction of the z-axis. We take $H_{a(n)}^{A(B)}$ to be $H_{a(1)}^{A(B)}$ on the surface and $H_a^{A(B)}$ otherwise. The summation in (2.1) is over all distinct pairs.

We define the spin-lowering operators $S_\ell^{\pm(\lambda)} = (1/\sqrt{2})(S_\ell^{X(\lambda)} \pm \mathrm{i} S_\ell^{Y(\lambda)})$ with $\lambda = \mathrm{A}$ or B. Due to the 2D periodicity of the surface layer, we define the wave vector $k_\parallel = (k_x, k_y)$

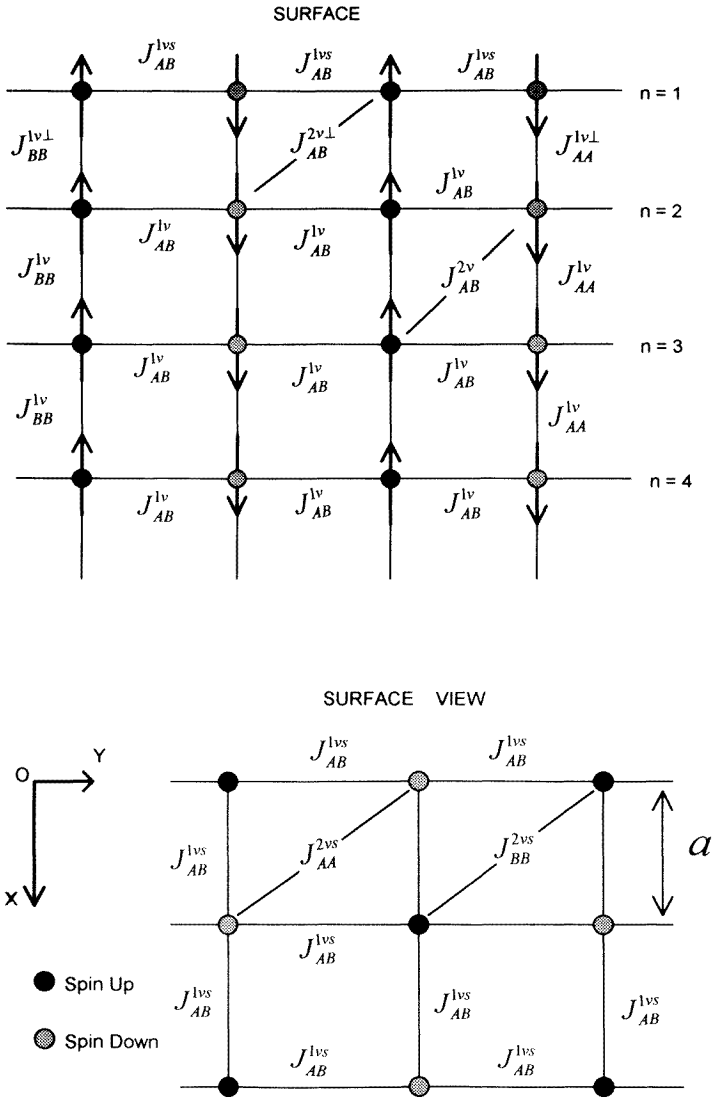

Figure 2. The (001) surface of a simple cubic superantiferromagnet. Beyond the second layer, all exchange interactions have the bulk value $J_{AB}^{1(2)v}(i,j)$ for antiferromagnetic inter-sublattice (A–B) nearest and next-nearest neighbours, and $J_{AA(BB)}^{1v}(i,i'(j,j'))$ for ferromagnetic intra-sublattice (A–A (B–B)) nearest neighbours only. The nearest- and the next-nearest-neighbour exchange interactions between spins on the surface were respectively defined by $J_{AB}^{1vs}(i,j)$ and $J_{AA(BB)}^{2vs}(i,i'(j,j'))$, and the interaction between the first and second layers by $J_{AB}^{2v\perp}(i,j)$ and $J_{AA(BB)}^{1v\perp}(i,i'(j,j'))$, respectively.

in the reciprocal space, and the operators $\alpha_{k_\parallel}^{+}$, $\beta_{k_\parallel}^{+}$ for each sublattice as

$$\begin{aligned} \alpha_{k_\parallel}^{+} &= \sum_{\langle i\rangle} S_i^{+(A)} \mathrm{e}^{-\mathrm{i}k_\parallel r_i} \qquad \text{and} \qquad S_i^{+(A)} = \sum_{\langle k\rangle} \alpha_{k_\parallel}^{+} \mathrm{e}^{-\mathrm{i}k_\parallel r_i} \\ \beta_{k_\parallel}^{+} &= \sum_{\langle j\rangle} S_j^{+(B)} \mathrm{e}^{-\mathrm{i}k_\parallel r_j} \qquad \text{and} \qquad S_j^{+(B)} = \sum_{\langle k\rangle} \beta_{k_\parallel}^{+} \mathrm{e}^{-\mathrm{i}k_\parallel r_j}. \end{aligned} \tag{2.2}$$

r_i and r_j denote the i- and j-atom vector positions on the x–y plane, respectively. The equation of motion $\mathrm{i}\hbar\ \mathrm{d}S_\ell^+/\mathrm{d}t = [S_\ell^+, H]$ leads to a two-sublattice system:

$$\begin{aligned} \mathrm{i}\hbar\dot{\alpha}_{k_\parallel}^+ &= D_{11}\alpha_{k_\parallel}^+ + D_{12}\beta_{k_\parallel}^+ \\ \mathrm{i}\hbar\dot{\beta}_{k_\parallel}^+ &= D_{21}\alpha_{k_\parallel}^+ + D_{22}\beta_{k_\parallel}^+ \end{aligned} \tag{2.3}$$

where the $D_{\sigma\xi}(\hbar\omega, J_{AB}^{1(2)v}, J_{AA(BB)}^{2v}, z_{ij}^{1(2)v}, z_{ii'(jj')}^{1(2)v}, S_{A(B)}, H_n^{A(B)})$ are given in appendix 1. Here $z_{ij}^{1(2)v}$ represents the inter-sublattice (A–B) number of nearest- and the second-nearest-neighbour atoms, respectively, and $z_{ii(jj)}^{1(2)v}$ corresponds to the intra-sublattice (A–A (B–B)) numbers.

In order to introduce the amplitude of precessional spin waves, the two-dimensional spatial Fourier transform operator $L^{(\lambda)}(R,\omega)$ was defined by

$$L^{(\lambda)}(R_{i(j)},\omega) = (2\pi a)^{-2}\int \mathrm{d}k_\parallel\ \exp(\mathrm{i}k_\parallel\eta_{i(j)})U_{n(R_{i(j)})}^{(\lambda)}(k_\parallel,\omega) \qquad (n \geqslant 1) \tag{2.4}$$

with $L^{(\lambda)} = \alpha_{k_\parallel}^+$ $(\beta_{k_\parallel}^+)$ if λ = A (B), and the quantities $U_{n(R_{i(j)})}^{(\lambda)}(k_\parallel,\omega)$ are spin-wave amplitudes for the λth-sublattice atom i (j) on the nth layer located at $R_{i(j)}$. The surface corresponds to the layer labelled by $n = 1$. Here the notation is such that $R_{i(j)} = (\eta_{i(j)}, na)$, where $\eta_{i(j)}$ is a two-dimensional position vector of the atom i (j) in the x–y plane, and na is the coordinate position normal to the surface (a is the layer spacing). The inter-sublattice (A–B) and intra-sublattice (A–A (B–B)) nearest- and the next-nearest-neighbour vectors are denoted by $\Delta_{ij}^{1(2)v}$ and $\Delta_{ii'(jj')}^{1(2)v}$, respectively.

Introducing the following parameters:

$$\begin{aligned} E &= \frac{\hbar\omega - g\mu_b H_0}{J_{AB}^{1vs}S} \\ \varepsilon_{ij}^{1v\parallel} &= \frac{J_{AB}^{1vs}}{J_{AB}^{1v}} \qquad \varepsilon_{ii'(jj')}^{2v\parallel} = \frac{J_{AA(BB)}^{2vs}}{J_{AB}^{1v}} \qquad \varepsilon_{ii'(jj')}^{2v} = \frac{J_{AA(BB)}^{2v}}{J_{AB}^{1v}} \qquad \varepsilon_{ii'(jj')}^{1v} = \frac{J_{AA(BB)}^{1v}}{J_{AB}^{1v}} \\ \varepsilon_{ii'(jj')}^{1v\perp} &= \frac{J_{AA(BB)}^{1v\perp}}{J_{AB}^{1v}} \qquad \varepsilon_{ii'(jj')}^{1v} = \frac{J_{AA(BB)}^{1v}}{J_{AB}^{1v}} \qquad \varepsilon_{ij}^{2v} = \frac{J_{AB}^{2v}}{J_{AB}^{1v}} \qquad \varepsilon_{ij}^{2v\perp} = \frac{J_{AB}^{2v\perp}}{J_{AB}^{1v}}. \end{aligned} \tag{2.5}$$

The equations for the spin-wave amplitude of each nth sublattice layer, which are obtained from equations (2.3), (2.4) and (2.5), can be written in the matrix form

$$\left[M^b\right]\left|U_n^{(\lambda)}\right\rangle = |0\rangle \tag{2.6}$$

where the matrix elements $M_{\sigma\xi}^b(E, J_{AB}^{1vs}, J_{AB}^{1(2)v}, J_{AA(BB)}^{1(2)v}, \varepsilon_{uw}, \varepsilon_{uw}^{1(2)v\parallel}, \varepsilon_{uw}^{1(2)v\perp}, \gamma_{pq}^{1(2)v(\parallel,\perp)}(k_\parallel), H_{a(n)}^{A(B)})$ are given in appendix 2, and $\left|U_n^{(\lambda)}\right\rangle$ is the vector column defined by

$$\left|U_n^{(\lambda)}\right\rangle = \begin{bmatrix} U_1^{(A)} \\ U_1^{(B)} \\ U_2^{(A)} \\ U_2^{(B)} \\ \cdot \\ \cdot \\ U_n^{(A)} \\ U_n^{(B)} \\ \cdot \end{bmatrix}.$$

The coefficients $\gamma_{pq}^{1v\|(\perp)}(k_\|)$ and $\gamma_{pq}^{2v\|(\perp)}(k_\|)$ are as follows:

$$\begin{aligned}
\gamma_{ij}^{1v\|}(k_\|) &= \frac{1}{z_{ij}^{1v\|}} \sum_{\langle \Delta_{ij}^{1v\|} \rangle} \mathrm{e}^{\mathrm{i}k_\| \Delta_{ij}^{1v\|}} = \frac{1}{2}\left[\cos(k_x a) + \cos(k_y a)\right] \\
\gamma_{ii'(jj')}^{1v\perp}(k_\|) &= \frac{1}{z_{ii(jj)}^{1v\perp}} \sum_{\langle \Delta_{ii(jj)}^{1v\perp} \rangle} \mathrm{e}^{\mathrm{i}k_\| \Delta_{ii(jj)}^{1v\perp}} = 1 \\
\gamma_{ii'(jj')}^{2v\|}(k_\|) &= \frac{1}{z_{ii(jj)}^{2v\|}} \sum_{\langle \Delta_{ii(jj)}^{1v\|} \rangle} \mathrm{e}^{\mathrm{i}k_\| \Delta_{ii(jj)}^{1v\|}} = \frac{1}{2}\left[\cos(k_x + k_y)a + \cos(k_x - k_y)a\right] \\
\gamma_{ij}^{2v\perp}(k_\|) &= \frac{1}{z_{ij}^{2v\perp}} \sum_{\langle \Delta_{ij}^{2v\perp} \rangle} \mathrm{e}^{\mathrm{i}k_\| \Delta_{ij}^{2v\perp}} = \frac{1}{2}\left[\cos(k_x a) + \cos(k_y a)\right].
\end{aligned} \tag{2.7}$$

In obtaining equation (2.6), we have employed a random-phase approximation and replaced $S_{i(j)}^Z$ by its thermal expectation value. At absolute zero, $T = 0$, all of the quantities $\langle S_n^Z \rangle \to S$, where S is the magnitude of the spin of the magnetic ion. At low temperatures, the departure of $\langle S^Z \rangle$ from S, due to thermal excitation of spin waves, is small. In this temperature range, $\langle S_n^Z \rangle$ is approximately uniform, except near the surface. Mills and Maradudin [13] have concluded that the deviation $\Delta_n = S - \langle S_n^Z \rangle$ is twice as large for the surface spins ($n = 1$) as for the bulk spins ($n \to \infty$). The principal result of this spatial variation in $\langle S_n^Z \rangle$ is to produce an effect similar to a weakening of the exchange constants at the surface. As the temperature increases, the effect of the surface on the spatial variation of the magnetization becomes more important. The numbers of layers whose magnetization is substantially lower than that of the bulk increases with increasing temperature. In this work, we shall limit our discussion to $T = 0$, for which $\langle S_n^Z \rangle = S$ for all n.

3. Model surface spin waves

Let us consider the (001) surface of a semi-infinite superantiferromagnetic lattice with $|S_A| = |S_B| = 5/2$ (see figure 2). Thus each atomic spin site i (j) of each corresponding λ-sublattice will be described by two integers $(\eta_{i(j)}, na)$ as previously defined.

In general, the precessional amplitude field of quantum spins in the bulk region ($n \geqslant 3$) can be described from group theory, including the translation operator properties [12, 14] via a general linear development on a complete set of the evanescent and bulk $(n_e + n_b)$ modes:

$$U(n, \lambda) = \sum_{\zeta=1}^{n_e+n_b} P_\zeta C(\lambda, \rho_\zeta) \rho^{n-3}(E, k_\|, \zeta) \tag{3.1}$$

where the weighting coefficients P_ζ characterize the contributions of different modes in the bulk precessional amplitude field, and the $C(\lambda, \rho_\zeta)$ are the corresponding polarization vectors which represent the cofactor of the (2×2) dynamical matrix D obtained from the previous expression, equation (2.3), with the condition

$$\sum_{\zeta=1}^{n_e+n_b} \left|C(\lambda, \rho_\zeta)\right|^2 = 1. \tag{3.2}$$

Owing to the 2D periodic character established by the mean-field approximation for the surface region, a wave vector $k_\|$ characterizes a two-dimensional Brillouin magnetic cell. Using the quantities $\varphi_x = k_x a$, $\varphi_y = k_y a$ and $\rho = \mathrm{e}^{\mathrm{i}k_z a}$, a set of evanescent modes in the

bulk region is obtained using equation (2.3) such that the matrix determinant $\det(D) = 0$, which leads to a polynomial $\psi(\rho)$ equation form, giving:

$$\psi\left[\rho(E, J_{AB}^{1(2)v}, J_{AA(BB)}^{1(2)v}, \phi_x, \phi_y, z_{ij}^{1(2)v}, z_{ii(jj)}^{1(2)v}, S_{A(B)}, H_n^{A(B)})\right] = 0. \tag{3.3}$$

Satisfying equation (3.3), there exists a trivial solution which results from the secular equation of the fourth degree in ρ. Both phase factors ρ and ρ^{-1} are solutions, because this system is Hermitian. We can then obtain a trivial solution which yields a ρ-secular equation, in which for each point in the space $(E, k_\parallel)$, there are four pairs of roots (ρ, ρ^{-1}), with n_b roots ρ such that $|\rho| = 1$ describes the projected bulk magnon modes on the surface, represented by the shaded area in the figures plotted, and n_e roots ρ such that $|\rho| < 1$ describes evanescent modes. The space $(E, k_\parallel)$ is hence divided into bulk magnon bands $(n_b > 0)$, and zones $(n_b < 0)$ within which the density of states of bulk magnons vanishes. The roots ρ for which $|\rho| > 1$, which give divergent solutions at infinity, are not taken into account in the present analysis.

The analysis of surface magnon branches requires the knowledge of the complete set of evanescent modes in the bulk region. These can be characterized by a complex phase factor which describes the decrease of the precessional amplitude with increasing penetration into the crystal [12]. Denoting this factor in the normal direction to the surface as ρ, the bulk and evanescent modes of magnons can be characterized by $|\rho| = 1$ and $|\rho| < 1$, respectively.

Denoting the vector composed by the coefficients P_ζ introduced above as $|P\rangle$, and the vector composed via a choice of a set of six consecutive components $U_n^{(\lambda)}$ of the surface and matching regions $(1 \leqslant n \leqslant 3)$ as $|U^{(\lambda)}\rangle$, and using equation (3.1), one obtains the matrix equations

$$|U^{(\lambda)}\rangle = \left[A(E, \varepsilon_{uw}^{1(2)v}, \gamma_{pq}^{1(2)v(\parallel,\perp)}(k_\parallel, \rho_\zeta), C(\lambda, \rho_\zeta)\right]|P\rangle \tag{3.4}$$

$$|P\rangle = \left[A(E, \varepsilon_{uw}^{1(2)v}, \gamma_{pq}^{1(2)v(\parallel,\perp)}(k_\parallel, \rho_\zeta), C(\lambda, \rho_\zeta)\right]^{-1}|U^{(\lambda)}\rangle \tag{3.5}$$

where $[A]$ is a (4×4) matrix whose elements $A_{\sigma\xi}(E, \varepsilon_{uw}^{1(2)v}, \gamma_{pq}^{1(2)v(\parallel,\perp)}(k_\parallel, \rho_\zeta), C(\lambda, \rho_\zeta))$ are deduced using equation (3.1). Thus, on successively applying (3.4) in the linear system (3.3) for the components $U_n^{(\lambda)}$, and then (3.5) to eliminate the coefficients P_ζ, the linear homogeneous system becomes

$$[E^2 I - M^s(\vartheta, \kappa, \{\rho\})]|U_n^{(\lambda)}\rangle = |0\rangle \tag{3.6}$$

where I is the unit matrix and

$$\vartheta, \kappa = \phi^{(\lambda)}(J_{AB}^{1vs}, J_{AB}^{1(2)v}, J_{AA(BB)}^{1(2)v}, \varepsilon_{uw}, \varepsilon_{uw}^{1(2)v\parallel}, \varepsilon_{uw}^{1(2)v\perp}, \gamma_{pq}(k_\parallel, \rho), E).$$

In equation (3.6), $|U_n^{(\lambda)}\rangle$ is a vector amplitude of the sublattice λ on the nth layer near the surface and matching regions, $M^s(\vartheta, \kappa)$ is a (6×6) mean dynamical matrix which describes the spin-wave dynamics of the system, and $\{\rho\}$ is a set of the $\zeta = 1, 2, \ldots, n_e + n_b$ roots $\rho(E, J_{AB}^{1(2)v}, J_{AA(BB)}^{1(2)v}, \varphi_x, \varphi_y, S_{A(B)}, H_n^{A(B)})$ given by the ρ-secular equation (3.3), in the $(E, k_\parallel)$ space. A non-trivial solution $|U_n^{(\lambda)}\rangle$ requires that the determinant of this system vanishes, which defines an algebraic equation in E, whose real and positive solutions $E_s(k_\parallel)$ yield the mean surface magnon branches in the n_b-zones, and the surface resonances in the zones where $n_b \neq 0$. Consequently, the localized states of magnons can be calculated also when the determinant system (3.6) vanishes:

$$\det(M^s) = 0. \tag{3.7}$$

The matrix elements M^s are developed in appendix 3.

$$\frac{J^{1v}_{AB}}{J^{2v}_{AA(BB)}} = 1$$

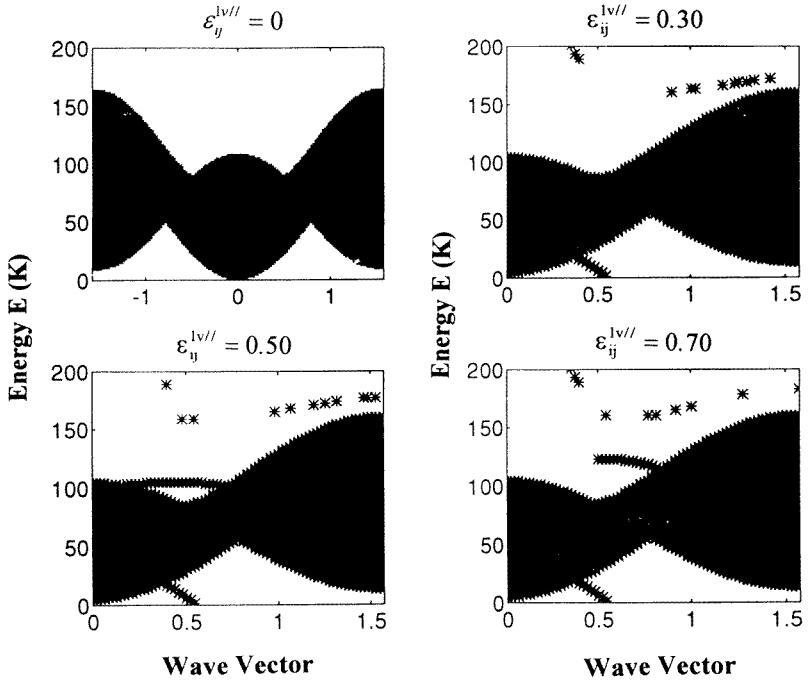

Figure 3. Energies of bulk and surface spin waves for $J^{1v}_{AB}/J^{2v}_{AA(BB)} = 1$ plotted in the [110] surface direction. The variation of the acoustic and optical modes at the surface relative to the bulk magnon domain is given as a function of the ratio $\varepsilon_{ij}^{1v\|} = J^{1vs}_{AB}/J^{1v}_{AB}$.

4. Numerical results and discussion

In the present paper, the localized energy states for the surface magnons were calculated in the [110] direction for the first bidimensional magnetic cell. The evolutions of surface magnons are reported in figures 3 to 5 as functions of the exchange bulk–surface ratio $\varepsilon_{ij}^{1v\|}$ to the values of the frustration parameter $J^{1v}_{AB}/J^{2v}_{AA(BB)} = 1, 3, 4$. The matching technique shows that the surface eigenstates exist within the bulk continuum of states. An excitation corresponding to a point $(E^0, k^0_\|)$ in the continuum which is localized near the surface would decay rapidly into non-local bulk-type states. The surface states change their magnetic character at critical values of $\varepsilon_{ij}^{1v\|}$ which strongly depend on the nature of the exchange coupling between the (A–B) nearest and the (A–A (B–B)) next-nearest neighbours. We may therefore omit the term for the effective field in the present calculations. For the sake of simplicity: (i) we consider the 'free-surface model', in which the exchange coupling constants ($J^{2v\perp}_{AB}$ and $J^{1v\perp}_{AA(BB)}$) near the surface are assumed to be the same as those of the bulk; and (ii) except the variations of $\varepsilon_{ij}^{1v\|}$, other data defined by equation (2.5) are assumed to be constant in the numerical procedure. Meanwhile, these parameters are considered in

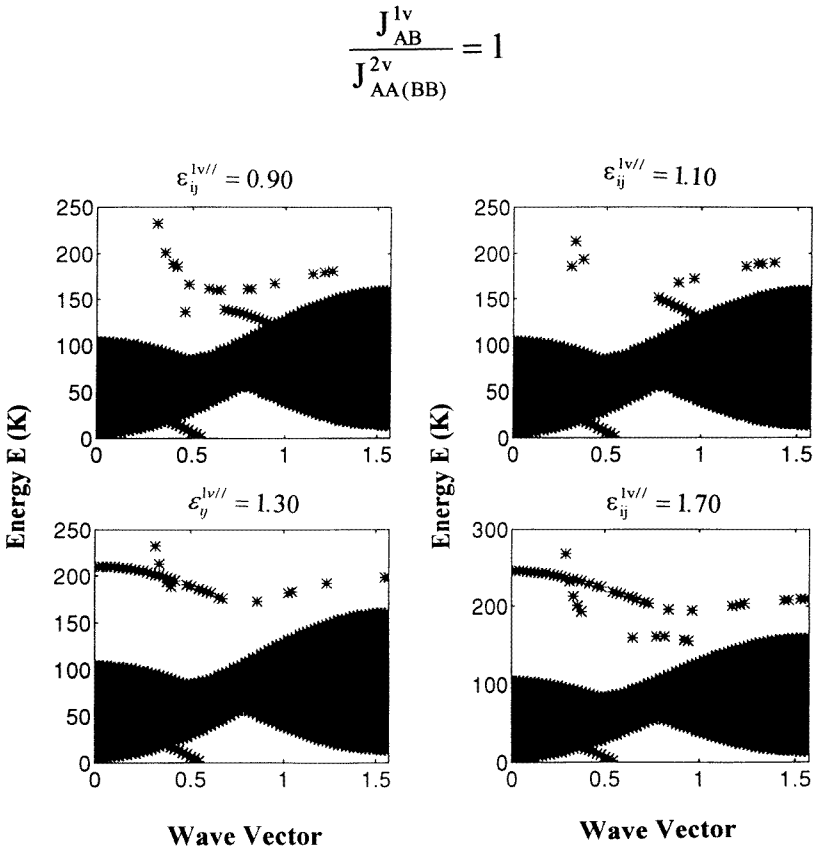

Figure 3. (Continued)

the analytical equations.

When $J^{1v}_{AB}/J^{2v}_{AA(BB)} = 1$ (see figure 3, assuming weak values of J^{1v}_{AB}), the surface acoustic modes are not energetic enough, in comparison with other values of the $J^{1v}_{AB}/J^{2v}_{AA(BB)}$ ratio (see figures 4 and 5), but the optical modes occur for $\varepsilon_{ij}^{1v\|} = 0.50$ and their energy increases with the increasing surface exchange value J^{1vs}_{AB}. The acoustic surface magnon mode remains independent of the $\varepsilon_{ij}^{1v\|}$-ratio for low energy. According to the evolutions of the constraint function illustrated in figure 1 and the bulk and surface eigenstate solutions, one can conclude that the superantiferromagnetic ground state is more pronounced than for other values of $J^{1v}_{AB}/J^{2v}_{AA(BB)}$ (see figures 4 and 5). On the other hand, the two optical modes obtained for $\varepsilon_{ij}^{1v\|} = 1.70$ exhibit a negative slope, and their intersection point confirms that the precession mode of these two magnons is not degenerate within this energy range. In addition, the acoustic mode which appears and touches zero frequency at a wave vector near 0.5 characterizes the clockwise precessional motion of the spin, without degeneracy, and explains the existence of the surface magnetic anisotropy. This feature was not observed for the antiferromagnetic ground-state Heisenberg system corresponding to the domain range values $J^{1v}_{AB}/J^{2v}_{AA(BB)} < 0$ and $J^{1v}_{AB}/J^{2v}_{AA(BB)} > 4$ [15]. The most interesting result is that when the spin layer draws near the surface, the spin magnetization rotates; this is similar to the 'pseudohelicoidal' phenomena in the vicinity of the surface. The

$$\frac{J^{1v}_{AB}}{J^{2v}_{AA(BB)}} = 3$$

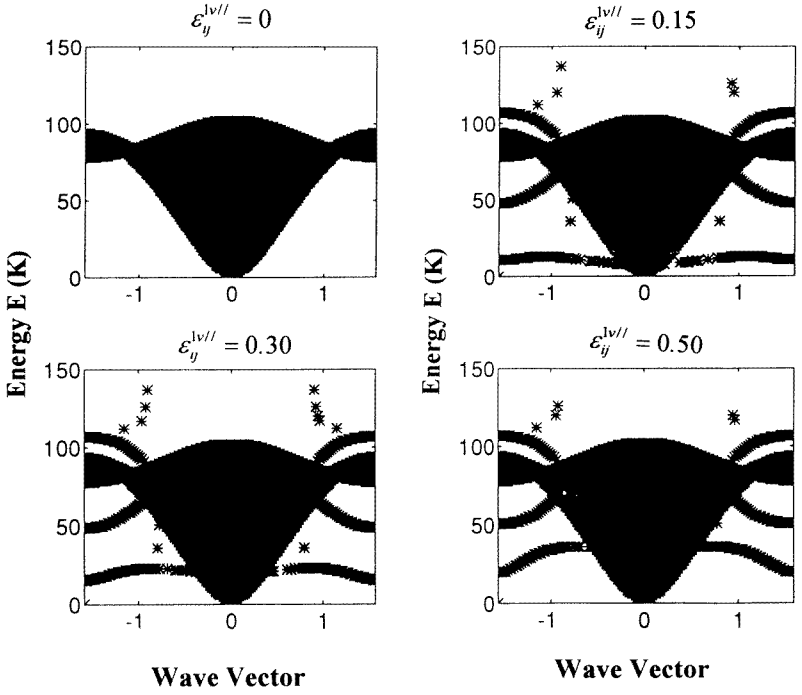

Figure 4. Energies of bulk and surface spin waves for $J^{1v}_{AB}/J^{2v}_{AA(BB)} = 3$ plotted in the [110] surface direction. The variation of the acoustic and optical modes at the surface relative to the bulk magnon domain is given as a function of the ratio $\varepsilon_{ij}^{1v\parallel} = J^{1vs}_{AB}/J^{1v}_{AB}$.

equilibrium orientation of the magnetization in the layers which are near the surface is tilted away from the direction of the magnetization in the bulk.

For $J^{1v}_{AB}/J^{2v}_{AA(BB)} = 3$ (figure 4), the acoustic modes which are energetic enough display a 'cut-off' and a negative slope. Their energies increase with increasing values of J^{1vs}_{AB}, and their negative slope is evident for values $\varepsilon_{ij}^{1v\parallel} \geqslant 0.5$. The two degenerate solutions correspond to the two opposite-spin surface precessions. For the values of $\varepsilon_{ij}^{1v\parallel} \geqslant 1.30$, these modes belong to the shaded area which represents the bulk modes projected on the (001) surface: one can observe the occurrence of an optical mode with negative slope when $\varepsilon_{ij}^{1v\parallel} \geqslant 1.30$ which allows the estimation of the Larmor frequency of spin precession. Furthermore, two degenerate optical branches appear for $\varepsilon_{ij}^{1v\parallel} = 1.30$. For one of these modes, because its energy is maximal at $k_\parallel = 0$, the existence of a magnetostatic mode can be deduced. This mode enters in the bulk band in order to appear in acoustic solution form; this feature is attributed to the anisotropic ratio defined from the surface anisotropy and the bulk exchange coupling originating from the broken symmetry of the surface [16]. The configuration of the transverse magnetization at the surface plane is present. The two kinds

$$\frac{J^{1v}_{AB}}{J^{2v}_{AA(BB)}} = 3$$

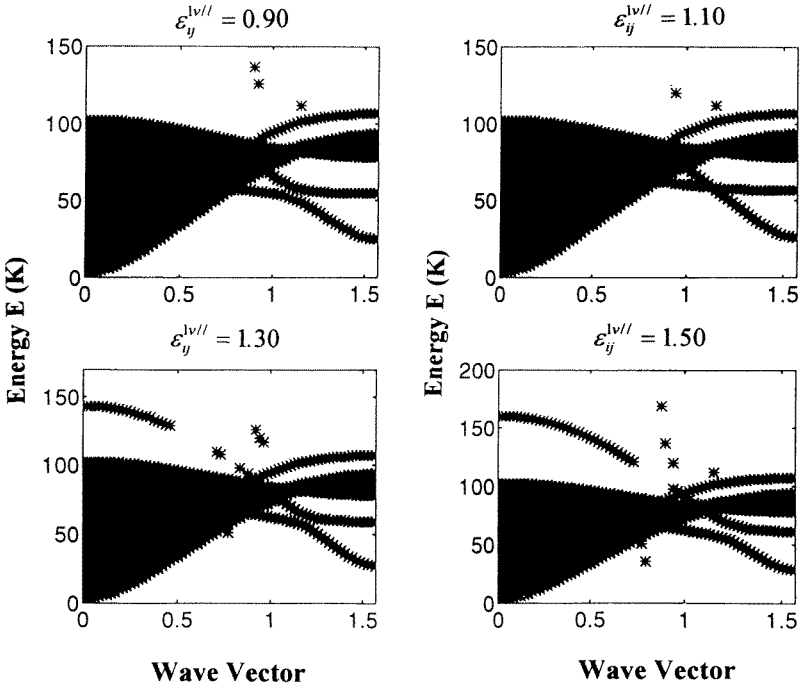

Figure 4. (Continued)

of optical surface magnon mode correspond to clockwise and anticlockwise precessional motions of spins, but are degenerate. This is reasonable, because the surface layer is equally probably occupied by up and down spins. Consequently, the surface spin arrangement displays different degenerate configurations of minimum energy; the disappearance of the optical mode with negative slope for $\varepsilon_{ij}^{1v\|} \leqslant 1.10$ is consistent with a canted surface magnetization in this domain range which cannot be clearly estimated.

For $J_{AB}^{1v}/J_{AA(BB)}^{2v} = 4$ (figure 5), we observe a complete disappearance of the superantiferromagnetic ground state, according to the previous results of computer simulations. The bulk magnon dispersion curves do not exhibit a negative slope near the edge of the Brillouin zone. For all values of $\varepsilon_{ij}^{1v\|}$, we obtain the classical solution of an optical mode which intersects the bulk magnon band, then at $\varepsilon_{ij}^{1v\|} = 1.30$ a magnetostatic mode appears with increasing energy when $\varepsilon_{ij}^{1v\|}$ increases. Two truncated acoustic modes occur for $\varepsilon_{ij}^{1v\|} \geqslant 0.50$. These modes touch zero frequency near the edge of the Brillouin zone. One finds that for one of the acoustic branches the point of truncation moves to larger $k_\|$ which corresponds to the unstable arrangement of spins at the surface.

Let us mention that for the bulk magnon band energy ($\varepsilon_{ij}^{1v\|} = 0$), the symmetry gauge is broken for $J_{AB}^{1v}/J_{AA(BB)}^{2v} = 1$ and less pronounced for $J_{AB}^{1v}/J_{AA(BB)}^{2v} = 3$, according to the

$$\frac{J^{1v}_{AB}}{J^{2v}_{AA(BB)}} = 4$$

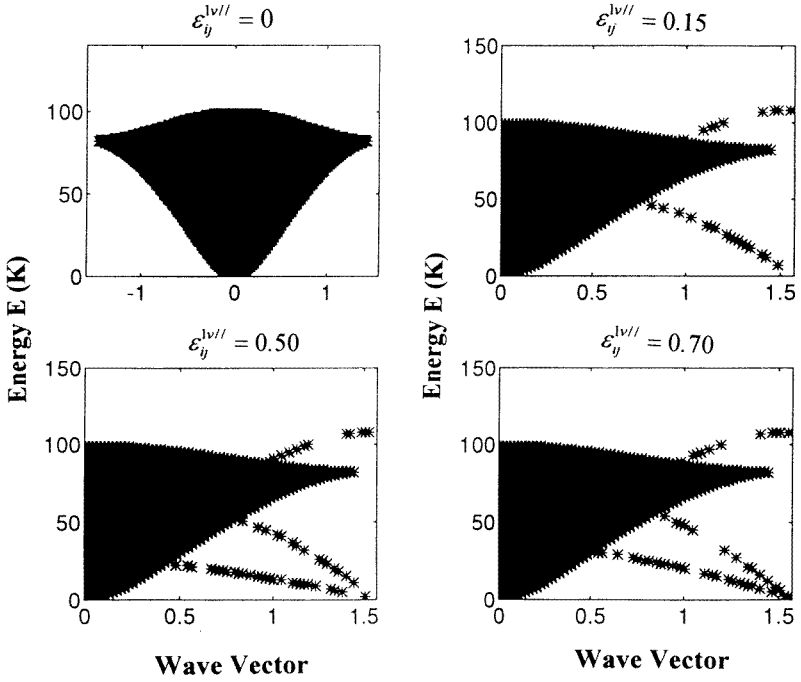

Figure 5. Energies of bulk and surface spin waves for $J^{1v}_{AB}/J^{2v}_{AA(BB)} = 4$ plotted in the [110] surface direction. The variation of the acoustic and optical modes at the surface relative to the bulk magnon domain is given as a function of the ratio $\varepsilon_{ij}^{1v\parallel} = J^{1vs}_{AB}/J^{1v}_{AB}$.

previous results concerning the infinite cubic systems when we consider a fully frustrated lattice with simultaneous ferro- and antiferromagnetic bonds [17]. For $J^{1v}_{AB}/J^{2v}_{AA(BB)} = 4$, a new physical solution appears, which confirms the new ground-state antiferromagnetic structure as previously described in a recent paper [15]. The evolutions of the acoustic modes in the domain range $0 < J^{1v}_{AB}/J^{2v}_{AA(BB)} \leqslant 4$ show that their solutions permit one to obtain the spin equilibrium position at a surface. Nevertheless, an important question which remains open is that of the direction of the magnetization at the surface in this structure.

5. Conclusion

In conclusion, this paper gives an illustration of the influence of the magnetic frustration parameter $J^{1v}_{AB}/J^{2v}_{AA(BB)}$ on the dispersion curves at the surface and in the bulk, assuming exchange bulk–surface interactions $\varepsilon_{ij}^{1v\parallel}$. The curvature of the bulk and surface spin-wave dispersion curves observed in the $0 < J^{1v}_{AB}/J^{2v}_{AA(BB)} \leqslant 4$ range illustrates an unstable rearrangement of spins in the structure. The magnetic phase transition at $J^{1v}_{AB}/J^{2v}_{AA(BB)} = 4$, which was predicted by computer simulation, was confirmed in this study. Consequently,

$$\frac{J^{1v}_{AB}}{J^{2v}_{AA(BB)}} = 4$$

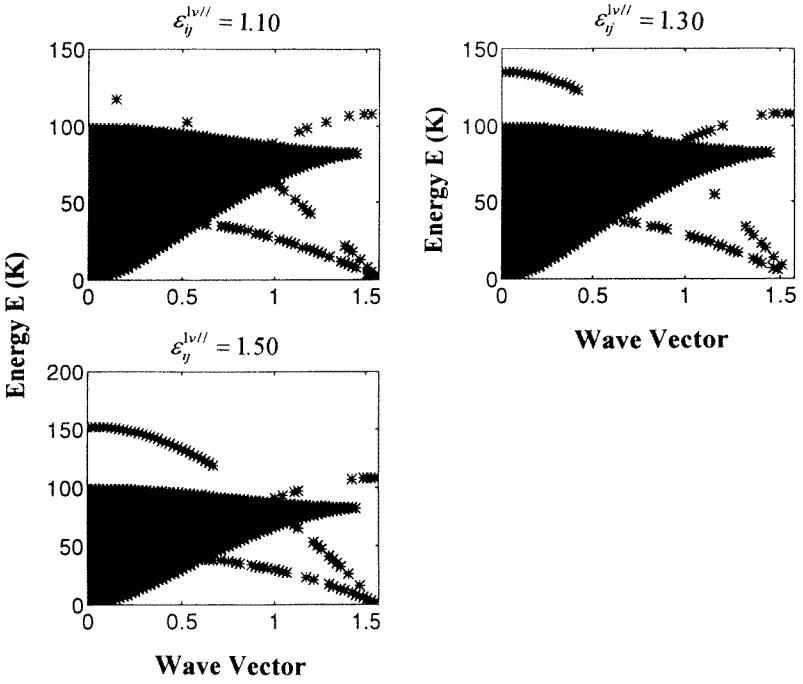

Figure 5. (Continued)

by assuming these results to be correct, one can calculate the surface magnetic behaviour of the other crystalline phases of FeF_3.

Further investigations of frustrated cubic superferrimagnets with $|S_A| \neq |S_B|$ are in progress with the aim of applying this theory to $Fe_{1-x}M_xF_3$ compounds (M = Cr, V, Mn, ...). This methodology can be used to describe the case of topologically frustrated systems with triangular spin lattices in order to explain the surface magnetic properties. On the other hand, this work is now being extended to amorphous phases which exhibit speromagnetic behaviour and for which some structural networks based upon a continuous random packing of corner-sharing octahedral units have been proposed [18, 19].

From the point of view of the theoretical aspects, the matching method, which was successfully applied to investigate the magnetic excitations on surface frustrated systems, gives evidence for the mean surface magnon dispersion curves. The results developed here can be completed, providing that the values of the surface effective field are known.

Acknowledgments

The author wishes to thank Professor Dr J M Greneche for many helpful discussions, and acknowledges a very useful correspondence with the referees, who are thanked for their remarks.

Appendix 1

The parameters $D_{11}, D_{12}, D_{21}, D_{22}$ given in equation (2.3) are defined as follows:

$$D_{11} = -z_{ij}^{1v}\langle S_B^Z\rangle \sum_{\langle i,j\rangle} J_{AB}^{1v}(i,j) + z_{ii'}^{1v}\langle S_A^Z\rangle \sum_{\langle i,i\rangle} J_{AA}^{1v}(i,i')\left\{\frac{1}{z_{ii'}^{1v}} e^{ik_\parallel (r_i - r_{i'})^{1v}} - 1\right\}$$
$$+ z_{ii'}^{2v}\langle S_A^Z\rangle \sum_{\langle i,i\rangle} J_{AA}^{2v}(i,i')\left\{\frac{1}{z_{ii}^{2v}} e^{ik_\parallel (r_i - r_{i'})^{2v}} - 1\right\}$$
$$- z_{ij}^{2v}\langle S_B^Z\rangle \sum_{\langle i,j\rangle} J_{AB}^{2v}(i,j) + \mu^{(A)} H_{(n)}^{(A)}$$

$$D_{12} = \langle S_A^Z\rangle \left[z_{ij}^{1v} \sum_{\langle i,j\rangle} J_{AB}^{1v}(i,j) \frac{1}{z_{ij}^{1v}} e^{ik_\parallel (r_i - r_j)^{1v}} + z_{ij}^{2v} \sum_{\langle i,j\rangle} J_{AB}^{2v}(i,j) \frac{1}{z_{ij}^{2v}} e^{ik_\parallel (r_i - r_j)^{2v}} \right]$$

$$D_{21} = \langle S_B^Z\rangle \left[z_{ij}^{1v} \sum_{\langle i,j\rangle} J_{AB}^{1v}(i,j) \frac{1}{z_{ij}^{1v}} e^{ik_\parallel (r_i - r_j)^{1v}} + z_{ij}^{2v} \sum_{\langle i,j\rangle} J_{AB}^{2v}(i,j) \frac{1}{z_{ij}^{2v}} e^{ik_\parallel (r_i - r_j)^{2v}} \right]$$

$$D_{22} = -z_{ij}^{1v}\langle S_A^Z\rangle \sum_{\langle i,j\rangle} J_{AB}^{1v}(i,j) + z_{jj'}^{1v}\langle S_B^Z\rangle \sum_{\langle j,j\rangle} J_{BB}^{1v}(j,j')\left\{\frac{1}{z_{jj}^{1v}} e^{ik_\parallel (r_j - r_{j'})^{1v}} - 1\right\}$$
$$+ z_{jj'}^{2v}\langle S_B^Z\rangle \sum_{\langle j,j\rangle} J_{BB}^{2v}(j,j')\left\{\frac{1}{z_{jj}^{2v}} e^{ik_\parallel (r_j - r_{j'})^{2v}} - 1\right\}$$
$$- z_{ij}^{2v}\langle S_A^Z\rangle \sum_{\langle i,j\rangle} J_{AB}^{2v}(i,j) + \mu^{(B)} H_{(n)}^{(B)}.$$

Appendix 2

The (6×8) matrix M^b given in the matching region $(1 \leqslant n \leqslant 4)$ is

$$[M^b] = \begin{bmatrix} M^b(1,1) & M^b(1,2) & . & . & 0 & 0 & 0 & 0 \\ M^b(2,1) & M^b(2,2) & \cdot & \cdot & 0 & 0 & 0 & 0 \\ \cdot & \cdot & \cdot & \cdot & \cdot & \cdot & 0 & 0 \\ \cdot & \cdot & \cdot & \cdot & \cdot & \cdot & 0 & 0 \\ 0 & 0 & \cdot & \cdot & \cdot & \cdot & \cdot & \cdot \\ 0 & 0 & \cdot & \cdot & M^b(6,5) & \cdot & \cdot & M^b(6,8) \end{bmatrix}$$

where the elements $M_{\sigma\xi}^b(E, J_{AB}^{1vs}, J_{AB}^{1(2)v}, J_{AA(BB)}^{1(2)v}, \varepsilon_{uw}, \varepsilon_{uw}^{1(2)v\parallel}, \varepsilon_{uw}^{1(2)v\perp}, \gamma_{pq}^{1(2)v(\parallel,\perp)}(k_\parallel), H_{a(n)}^{A(B)})$ are described by

$$M^b(1,1) = \left[E - \left(4\varepsilon_{ij}^{1v\parallel} + 4\varepsilon_{ij}^{2v\perp} + 4\varepsilon_{ii'}^{2v\parallel}(\gamma_{ii'}^{2v\parallel} - 1) - \varepsilon_{ii'}^{1v\perp} + \frac{g\mu_b}{JS} H_{a(1)}^{(A)} \right) \right]$$
$$M^b(1,2) = -M^b(2,1) = -4\varepsilon_{ij}^{1v\parallel}\gamma_{ij}^{1v\parallel}$$
$$M^b(1,3) = M^b(3,1) = -\varepsilon_{ii'}^{1v\perp}\gamma_{ii'}^{1v\perp}$$
$$M^b(1,4) = -M^b(4,1) = -M^b(2,3) = M^b(3,2) = -4\varepsilon_{ij}^{2v\perp}\gamma_{ij}^{2v\perp}$$
$$M^b(2,2) = \left[E + \left(4\varepsilon_{ij}^{1v\parallel} + 4\varepsilon_{ij}^{2v\perp} + 4\varepsilon_{jj'}^{2v\parallel}(\gamma_{jj'}^{2v\parallel} - 1) - \varepsilon_{jj'}^{1v\perp} - \frac{g\mu_b}{JS} H_{a(1)}^{(B)} \right) \right]$$
$$M^b(2,4) = M^b(4,2) = \varepsilon_{jj'}^{1v\perp}\gamma_{jj'}^{1v\perp}$$

$$M^b(3,3)=\left[E-\left(4-\varepsilon_{ii'}^{1v\perp}-\varepsilon_{ii}^{1v}+4\varepsilon_{ii'}^{2v}(\gamma_{ii'}^{2v\parallel}-1)+4\varepsilon_{ij}^{2v\perp}+4\varepsilon_{ij}^{2v}+\frac{g\mu_b}{JS}H_a^{(A)}\right)\right]$$
$$M^b(3,4)=-M^b(4,3)=M^b(5,6)=-M^b(6,5)=-4\gamma_{ij}^{1v\parallel}$$
$$M^b(3,5)=-M^b(5,3)=M^b(5,7)=\varepsilon_{ii}^{1v}\gamma_{ii'}^{1v\perp}$$
$$M^b(3,6)=-M^b(6,3)=-4\varepsilon_{ij}^{2v}\gamma_{ij}^{2v\perp}$$
$$M^b(4,4)=\left[E+\left(4-\varepsilon_{jj'}^{1v\perp}-\varepsilon_{jj'}^{1v}+4\varepsilon_{jj}^{2v}(\gamma_{jj'}^{2v\parallel}-1)+4\varepsilon_{ij}^{2v\perp}+4\varepsilon_{ij}^{2v}-\frac{g\mu_b}{JS}H_a^{(B)}\right)\right]$$
$$M^b(4,5)=-M^b(5,4)=-M^b(5,8)=M^b(6,7)=4\varepsilon_{ij}^{2v}\gamma_{ij}^{2v\perp}$$
$$M^b(4,6)=M^b(6,4)=M^b(6,8)=\varepsilon_{jj'}^{1v}\gamma_{jj'}^{1v\perp}$$
$$M^b(5,5)=\left[E-\left(4-2\varepsilon_{ii}^{1v}+4\varepsilon_{ii'}(\gamma_{ii'}^{2v\parallel}-1)+8\varepsilon_{ij}^{2v}+\frac{g\mu_b}{JS}H_a^{(A)}\right)\right]$$
$$M^b(6,6)=\left[E+\left(4-2\varepsilon_{jj'}^{1v}+4\varepsilon_{jj'}(\gamma_{jj'}^{2v\parallel}-1)+8\varepsilon_{ij}^{2v}-\frac{g\mu_b}{JS}H_a^{(B)}\right)\right].$$

Appendix 3

The fully square matrix M^s is as follows:

$$[M^s]=\begin{bmatrix} M^s(1,1) & M^s(1,2) & \cdot & \cdot & 0 & 0 \\ M^s(2,1) & M^s(2,2) & \cdot & \cdot & 0 & 0 \\ \cdot & \cdot & M^s(3,3) & \cdot & \cdot & \cdot \\ \cdot & \cdot & \cdot & \cdot & \cdot & \cdot \\ 0 & 0 & \cdot & \cdot & \cdot & \cdot \\ 0 & 0 & \cdot & \cdot & \cdot & M^s(6,6) \end{bmatrix}$$

where the elements $M^s_{\sigma\xi}(E, J^{1vs}_{AB}, J^{1(2)v}_{AB}, J^{1(2)v}_{AA(BB)}, \varepsilon_{uw}, \varepsilon^{1(2)v\parallel}_{uw}, \varepsilon^{1(2)v\perp}_{uw}, \gamma^{1(2)v(\parallel,\perp)}_{pq}(k_\parallel), H^{A(B)}_{a(n)})$ are given by

$$M^s(1,1)=\left[E-\left(4\varepsilon_{ij}^{1v\parallel}+4\varepsilon_{ij}^{2v\perp}+4\varepsilon_{ii'}^{2v\parallel}(\gamma_{ii'}^{2v\parallel}-1)-\varepsilon_{ii'}^{1v\perp}+\frac{g\mu_b}{JS}H_{a(1)}^{(A)}\right)\right]$$
$$M^s(1,2)=-M^s(2,1)=-4\varepsilon_{ij}^{1v\parallel}\gamma_{ij}^{1v\parallel}$$
$$M^s(1,3)=M^s(3,1)=-\varepsilon_{ii'}^{1v\perp}\gamma_{ii'}^{1v\perp}$$
$$M^s(1,4)=-M^s(4,1)=M^s(2,3)=-M^s(3,2)=-4\varepsilon_{ij}^{2v\perp}\gamma_{ij}^{2v\perp}$$
$$M^s(2,2)=\left[E+\left(4\varepsilon_{ij}^{1v\parallel}+4\varepsilon_{ij}^{2v\perp}+4\varepsilon_{jj'}^{2v\parallel}(\gamma_{jj'}^{2v\parallel}-1)-\varepsilon_{jj'}^{1v\perp}-\frac{g\mu_b}{JS}H_{a(1)}^{(B)}\right)\right]$$
$$M^s(2,4)=M^s(4,2)=\varepsilon_{jj'}^{1v\perp}\gamma_{jj'}^{1v\perp}$$
$$M^s(3,3)=\left[E-\left(4-\varepsilon_{ii'}^{1v\perp}-\varepsilon_{ii'}^{1v}+4\varepsilon_{ii'}^{2v}(\gamma_{ii'}^{2v\parallel}-1)+4\varepsilon_{ij}^{2v\perp}+4\varepsilon_{ij}^{2v}+\frac{g\mu_b}{JS}H_a^{(A)}\right)\right]$$
$$M^s(3,4)=-M^s(4,3)=-4\gamma_{ij}^{1v\parallel}$$
$$M^s(3,5)=-\left[\varepsilon_{ii'}^{1v}\gamma_{ii'}^{1v\perp}C(A,\rho_1)+4\varepsilon_{ij}^{2v}\gamma_{ij}^{2v\perp}C(B,\rho_1)\right]$$
$$M^s(3,6)=-\left[\varepsilon_{ii'}^{1v}\gamma_{ii'}^{1v\perp}C(A,\rho_2)+4\varepsilon_{ij}^{2v}\gamma_{ij}^{2v\perp}C(B,\rho_2)\right]$$
$$M^s(4,4)=\left[E+\left(4-\varepsilon_{jj'}^{1v\perp}-\varepsilon_{jj'}^{1v}+4\varepsilon_{jj'}^{2v}(\gamma_{jj'}^{2v\parallel}-1)+4\varepsilon_{ij}^{2v\perp}+4\varepsilon_{ij}^{2v}-\frac{g\mu_b}{JS}H_a^{(B)}\right)\right]$$
$$M^s(4,5)=+\left[\varepsilon_{jj'}^{1v}\gamma_{jj'}^{1v\perp}C(B,\rho_1)+4\varepsilon_{ij}^{2v}\gamma_{ij}^{2v\perp}C(A,\rho_1)\right]$$

$$M^s(4,6) = +\left[\varepsilon^{1v}_{jj'}\gamma^{1v\perp}_{jj'}C(B,\rho_2) + 4\varepsilon^{2v}_{ij}\gamma^{2v\perp}_{ij}C(A,\rho_2)\right]$$

$$M^s(5,3) = -\varepsilon^{1v}_{ii'}\gamma^{1v\perp}_{ii'}$$

$$M^s(5,4) = -M^s(6,3) = 4\varepsilon^{2v}_{ij}\gamma^{2v\perp}_{ij}$$

$$M^s(5,5) = \left[\left(E - \left(4 - 2\varepsilon^{1v}_{ii'} + 4\varepsilon^{2v}_{ii'}(\gamma^{2v\parallel}_{ii'} - 1) + 8\varepsilon^{2v}_{ij} + \frac{g\mu_b}{JS}H^{(A)}_a\right)\right)C(A,\rho_1) - 4\gamma^{1v\parallel}_{ij}C(B,\rho_1) - \varepsilon^{1v}_{ii'}\gamma^{1v}_{ii'}C(A,\rho_1)\rho_1 - 4\varepsilon^{2v}_{ij}\gamma^{2v\perp}_{ij}C(B,\rho_1)\rho_1\right]$$

$$M^s(5,6) = \left[\left(E - \left(4 - 2\varepsilon^{1v}_{ii'} + 4\varepsilon^{2v}_{ii'}(\gamma^{2v\parallel}_{ii'} - 1) + 8\varepsilon^{2v}_{ij} + \frac{g\mu_b}{JS}H^{(A)}_a\right)\right)C(A,\rho_2) - 4\gamma^{1v\parallel}_{ij}C(B,\rho_2) - \varepsilon^{1v}_{ii'}\gamma^{1v}_{ii'}C(A,\rho_2)\rho_2 - 4\varepsilon^{2v}_{ij}\gamma^{2v\perp}_{ij}C(B,\rho_2)\rho_2\right]$$

$$M^s(6,4) = \varepsilon^{1v}_{jj'}\gamma^{1v\perp}_{jj'}$$

$$M^s(6,5) = \left[\left(E + \left(4 - 2\varepsilon^{1v}_{jj'} + 4\varepsilon^{2v}_{jj'}(\gamma^{2v\parallel}_{jj'} - 1) + 8\varepsilon^{2v}_{ij} - \frac{g\mu_b}{JS}H^{(B)}_a\right)\right)C(B,\rho_1) + 4\gamma^{1v\parallel}_{ij}C(A,\rho_1) + \varepsilon^{1v}_{jj'}\gamma^{1v}_{jj'}C(B,\rho_1)\rho_1 + 4\varepsilon^{2v}_{ij}\gamma^{2v\perp}_{ij}C(A,\rho_1)\rho_1\right]$$

$$M^s(6,6) = \left[\left(E + \left(4 - 2\varepsilon^{1v}_{jj'} + 4\varepsilon^{2v}_{jj'}(\gamma^{2v\parallel}_{jj'} - 1) + 8\varepsilon^{2v}_{ij} - \frac{g\mu_b}{JS}H^{(B)}_a\right)\right)C(B,\rho_2) + 4\gamma^{1v\parallel}_{ij}C(A,\rho_2) + \varepsilon^{1v}_{jj'}\gamma^{1v}_{jj'}C(B,\rho_2)\rho_2 + 4\varepsilon^{2v}_{ij}\gamma^{2v\perp}_{ij}C(A,\rho_2)\rho_2\right].$$

References

[1] Derrida B, Pommeau Y, Toulouse G and Vannimenus J 1980 *J. Physique* **41** 213–21
[2] Villain J 1977 *J. Phys. C: Solid State Phys.* **10** 1717–34
[3] Choi M Y and Doniach S 1985 *Phys. Rev.* B **31** 4516–26
[4] Halsey T C 1985 *Phys. Rev.* B **31** 5728–45
[5] Coey J M D 1987 *Can. J. Phys.* **65** 1210–32
[6] Baltzer P, Wojtowicz P J, Robbins M and Lopatin E 1966 *Phys. Rev.* **151** 367–77
[7] Ramirez A P 1991 *J. Appl. Phys.* **70** 5952–5
[8] Ferey G, Leblanc M, Pannetier J and de Pape R 1985 *Inorganic Solid Fluorides* ed P Hagenmuller (New York: Academic) p 395
[9] Lacorre P, Pannetier J, Leblanc M and Ferey G 1991 *J. Magn. Magn. Mater.* **92** 366–74
[10] Tamine M and Greneche J M 1996 *Solid State Commun.* **98** 69–72
[11] Moran-Lopez J L, Aguilera-Granjand F and Sanchez J M 1994 *J. Phys.: Condens. Matter* **6** 9759–72
[12] Tamine M 1996 *J. Magn. Magn. Mater.* **153** 366–78
[13] Mills D L and Maradudin A A 1967 *J. Phys. Chem. Solids* **28** 1855–74
[14] Tinkham M 1964 *Group Theory and Quantum Mechanics* (New York: McGraw-Hill)
[15] Tamine M 1996 *Surf. Sci.* **346** 264–82
[16] Ilisca E and Gallais E 1972 *J. Physique* **33** 811–24
[17] Azaria P 1986 *J. Phys. C: Solid State Phys.* **19** 2773–83
[18] Coey J M D and Murphy P J K 1982 *J. Non-Cryst. Solids* **50** 125–9
[19] Greneche J M, Teillet J and Coey J M D 1986 *J. Non-Cryst. Solids* **83** 27–34